"Southwestern" boundary of the $N = 40$ island of inversion: First study of low-lying bound excited states in ^{59}V and ^{61}V

Z. Elekes,[1,2] M. M. Juhász,[1,2] D. Sohler,[1] K. Sieja,[3,4] K. Yoshida,[5] K. Ogata,[6,7] P. Doornenbal,[8] A. Obertelli,[8,9,10]
N. L. Achouri,[11] H. Baba,[8] F. Browne,[8] D. Calvet,[10] F. Château,[10] S. Chen,[8,12,13] N. Chiga,[8] A. Corsi,[10] M. L. Cortés,[8]
A. Delbart,[10] J.-M. Gheller,[10] A. Giganon,[10] A. Gillibert,[10] C. Hilaire,[10] T. Isobe,[8] T. Kobayashi,[14] Y. Kubota,[8,15] V. Lapoux,[10]
H. N. Liu,[9,10,16] T. Motobayashi,[8] I. Murray,[8,17] H. Otsu,[8] V. Panin,[8] N. Paul,[18] W. Rodriguez,[8,19,20] H. Sakurai,[8,21] M. Sasano,[8]
D. Steppenbeck,[8] L. Stuhl,[22,1] Y. L. Sun,[9,10] Y. Togano,[23] T. Uesaka,[8] K. Wimmer,[21,8] K. Yoneda,[8] O. Aktas,[16] T. Aumann,[9,24]
L. X. Chung,[25] Zs. Dombrádi,[1] F. Flavigny,[17] S. Franchoo,[17] I. Gašparić,[8,26] R.-B. Gerst,[27] J. Gibelin,[11] K. I. Hahn,[28,22]
D. Kim,[8,28,22] T. Koiwai,[21] Y. Kondo,[29] P. Koseoglou,[9,24] J. Lee,[13] C. Lehr,[9] B. D. Linh,[25] T. Lokotko,[13] M. MacCormick,[17]
K. Moschner,[27] T. Nakamura,[29] S. Y. Park,[30,31] D. Rossi,[9,24] E. Sahin,[32] P.-A. Söderström,[9,33] S. Takeuchi,[29] H. Törnqvist,[9,24]
V. Vaquero,[34] V. Wagner,[9] S. Wang,[35] V. Werner,[9,36] X. Xu,[13] H. Yamada,[29] D. Yan,[35] Z. Yang,[8] M. Yasuda,[29] and L. Zanetti[9]
(Sunflower Collaboration)

[1]*Atomki, P.O. Box 51, H-4001 Debrecen, Hungary*
[2]*University of Debrecen, Egyetem tér 1, H-4032 Debrecen, Hungary*
[3]*Université de Strasbourg, IPHC, 23 Rue du Loess 67037 Strasbourg, France*
[4]*CNRS, UMR7178, 67037 Strasbourg, France*
[5]*Advanced Science Research Center, Japan Atomic Energy Agency, Tokai, Ibaraki 319-1195, Japan*
[6]*Research Center for Nuclear Physics (RCNP), Osaka University, Ibaraki 567-0047, Japan*
[7]*Department of Physics, Kyushu University, Fukuoka 819-0395, Japan*
[8]*RIKEN Nishina Center, 2-1 Hirosawa, Wako, Saitama 351-0198, Japan*
[9]*Institut für Kernphysik, Technische Universität Darmstadt, 64289 Darmstadt, Germany*
[10]*IRFU, CEA, Université Paris-Saclay, F-91191 Gif-sur-Yvette, France*
[11]*LPC Caen, ENSICAEN, Université de Caen, CNRS/IN2P3, F-14050 Caen, France*
[12]*State Key Laboratory of Nuclear Physics and Technology, Peking University, Beijing 100871, People's Republic of China*
[13]*Department of Physics, The University of Hong Kong, Pokfulam Road, Hong Kong*
[14]*Department of Physics, Tohoku University, Sendai 980-8578, Japan*
[15]*Center for Nuclear Study, University of Tokyo, RIKEN campus, Wako, Saitama 351-0198, Japan*
[16]*Department of Physics, Royal Institute of Technology, SE-10691 Stockholm, Sweden*
[17]*IJCLab, IN2P3-CNRS, Université Paris-Saclay, 91405 Orsay Cedex, France*
[18]*Laboratoire Kastler Brossel, Sorbonne Université, CNRS, ENS-PSL Research University,*
Collège de France, Case 74, 4, Place Jussieu, 75005 Paris, France
[19]*Universidad Nacional de Colombia, Sede Bogota, Facultad de Ciencias, Departamento de Física, 111321 Bogotá, Colombia*
[20]*Pontificia Universidad Javeriana, Facultad de Ciencias, Departamento de Física, Bogotá 110231, Colombia*
[21]*Department of Physics, University of Tokyo, 7-3-1 Hongo, Bunkyo, Tokyo 113-0033, Japan*
[22]*Center for Exotic Nuclear Studies, Institute for Basic Science, Daejon 34126, Korea*
[23]*Department of Physics, Rikkyo University, 3-34-1 Nishi-Ikebukuro, Toshima, Tokyo 172-8501, Japan*
[24]*GSI Helmoltzzentrum für Schwerionenforschung GmbH, 64291 Darmstadt, Germany*
[25]*Institute for Nuclear Science & Technology, VINATOM, P.O. Box 5T-160, Nghia Do, Hanoi, Vietnam*
[26]*Ruđer Bošković Institute, Bijenička cesta 54, 10000 Zagreb, Croatia*
[27]*Institut für Kernphysik, Universität zu Köln, D-50937 Cologne, Germany*
[28]*Ewha Womans University, Seoul 03760, Korea*
[29]*Department of Physics, Tokyo Institute of Technology, 2-12-1 O-Okayama, Meguro, Tokyo 152-8551, Japan*
[30]*Ewha Womans University, Seoul 120-750, Korea*
[31]*Institute for Basic Science, Daejon 34126, Korea*
[32]*Department of Physics, University of Oslo, N-0316 Oslo, Norway*
[33]*Extreme Light InfrastructureNuclear Physics (ELI-NP)/Horia Hulubei National Institute for*
Physics and Nuclear Engineering (IFIN-HH), Str. Reactorului 30, 077125 Bucharest-Măgurele, Romania
[34]*Instituto de Estructura de la Materia, CSIC, E-28006 Madrid, Spain*
[35]*Institute of Modern Physics, Chinese Academy of Sciences, Lanzhou 730000, China*
[36]*Helmholtz Forschungsakademie Hessen für FAIR (HFHF), GSI Helmholtzzentrum für Schwerionenforschung,*
Campus Darmstadt, 64289 Darmstadt, Germany

The low-lying level structure of ^{59}V and ^{61}V was investigated for the first time. The neutron knockout reaction and inelastic proton scattering were applied for ^{61}V while the neutron knock-out reaction provided the data for ^{59}V. Four and five new transitions were determined for ^{59}V and ^{61}V, respectively. Based on the comparison to our shell-model calculations using the Lenzi-Nowacki-Poves-Sieja (LNPS) interaction, three of the observed γ rays for each isotope could be placed in the level scheme and assigned to the decay of the first $11/2^-$ and $9/2^-$ levels. The (p, p') excitation cross sections for ^{61}V were analyzed by the coupled-channels formalism assuming quadrupole plus hexadecapole deformations. Due to the role of the hexadecapole deformation, ^{61}V could not be unambiguously placed on the *island of inversion*.

I. INTRODUCTION

After the discovery of the first *island of inversion* among the neutron-rich nuclei near the $N = 20$ shell gap [1–6], more than twenty years ago the presence of another island was indicated near the $N = 40$ shell gap during the study of iron isotopes [7]. This was theoretically investigated [8] by introducing the Lenzi-Nowacki-Poves-Sieja (LNPS) interaction, and the *island* was suggested to lie around the region of $Z = 22$–26 and $N = 38$–42. In analogy to the *island of inversion* around $N = 20$, here the isotopic chains are characterized by open proton shells and the presence of neutron intruders $g_{9/2}d_{5/2}$ at low energy, thus quadrupole correlations can develop, maximizing the deformation at ^{64}Cr.

Therefore, this region came also into the focus of experiments including the cobalt [9,10], iron [11–13], manganese [14,15], chromium [16–18], and titanium [19–21] isotopes. For the $N = 40$ isotones, by removing protons from ^{68}Ni, the results showed an increase of collectivity up to ^{64}Cr (reaching a quadrupole deformation parameter β_2 of around 0.3 [13]), and a decrease toward the drip line in ^{63}V ($\beta_2 = 0.24$) [22]. The location of the first 2^+ state in ^{62}Ti suggested a further decrease of the deformation [20]. Going "west" from the center of the *island* to the $N = 38$ isotones, the measurements found $\beta_2 = 0.322$ for ^{62}Cr [23], and the energy of the 2_1^+ state in ^{60}Ti [19] compared to that of ^{62}Ti indicated the weakening of the collectivity. One step further at the $N = 36$ isotones, the quadrupole deformation parameter of ^{60}Cr was derived to be still large ($\beta_2 = 0.275$) [23] but that of ^{58}Ti was already obtained to be much smaller ($\beta_2 = 0.18$) [23].

However, little is known about the vanadium isotopes with neutron numbers 36 and 38 located between the isotopic chains of chromium and titanium. Therefore, we have studied the low-lying excited states of ^{59}V by the neutron knockout reaction and that of ^{61}V by proton inelastic scattering and the neutron knock-out reaction for the first time in order to shed some more light on the "southwestern" (low-N, low-Z) boundary of the *island of inversion* near the $N = 40$ shell gap.

II. EXPERIMENT

The experiment was carried out at the Radioactive Isotope Beam Factory operated by the RIKEN Nishina Center and the Center for Nuclear Study of the University of Tokyo. The secondary radioactive ion beam consisted of many nuclei with a range of the atomic number $Z = 17$–24 and that of the mass-to-charge ratio $A/Q = 2.5$–3.0, which provided a rich ground for new results published earlier. The details of the setup were discussed in the corresponding papers [20,22,24–31], therefore only some relevant parts were reviewed here, specific for the nuclei and reactions in question.

A beam of ^{70}Zn ions was produced at an energy of 345 MeV/u and at a beam intensity of 240 pnA by the accelerator complex. This primary stable beam collided with a ^{9}Be production target of 10 mm thickness, forming radioactive nuclei by fragmentation. The BigRIPS separator [32] was used to achieve a 5.5σ separation in Z and a 26.4σ separation in A/Q for the vanadium isotopes by the $B\rho$-ΔE-TOF method ($B\rho$: Magnetic rigidity, ΔE: Energy loss, TOF: Time of flight) [33]. The excited states of ^{59}V and ^{61}V were populated in the MINOS device [34] which consisted of a 151-mm-long cell filled with liquid hydrogen and a cylindrical time projection chamber (TPC). The point of reaction was reconstructed by using the scattered proton and the projected trajectory of the radioactive ions monitored by several sets of parallel plate avalanche counters (PPACs) [35]. An overall efficiency of 65% and a resolution of 5 mm (FWHM) along the beam axis were achieved. On average, the total, the ^{61}V, and the ^{62}V beam intensities were 200, 8, and 7 particles/s, respectively. The kinetic energies at the entrance of the target of the ^{61}V and ^{62}V particles were around 250 MeV/u, and the ions lost about 80 MeV/u passing through the liquid hydrogen.

The DALI2$^+$ array [36,37] of 226 NaI(Tl) scintillators detected the prompt γ rays. The beamlike fragments downstream of the target were analyzed by the SAMURAI spectrometer [38] based on $B\rho$, ΔE, and TOF measurements using multiwire drift chambers and a plastic scintillator wall of 24 bars. The unambiguous identification of the fragments was done by the multidimensional fit procedure of the ROOT framework [39], obtaining 8.9σ separation in Z and 7.8σ separation in A/Q.

For the observation of excited states decaying by neutron emission, neutron TOF spectrometers NeuLAND and NEB-ULA were placed at 11 and 14 m, respectively, downstream of the target at 0° [40]. NEBULA consisted of 120 plastic scintillator bars, each with a dimension of 12 cm(W) $\times$ 12 cm(D) $\times$ 180 cm(H) arranged in two walls. Both walls consisted of two layers and were equipped with an additional thin (1 cm) layer of plastic scintillators vetoing against the charged particles. The front face of the walls were separated by a distance of 85 cm. 400 NeuLAND units with a dimension of 5 cm(W) $\times$ 5 cm(D) $\times$ 250 cm(H) developed by the R^{3}B Collaboration

[41] were placed upstream of NEBULA in eight alternating horizontal and vertical layers to increase efficiency.

III. RESULTS AND DISCUSSION

The DALI2$^+$ detectors were calibrated for energy several times during the experiment, and only a minimal gain shift below 0.4% was observed. The photopeak efficiency of the setup was increased by the add-back procedure in the analysis by merging the hits in the adjacent units (<15 cm) in an event. The γ rays were also Doppler corrected for the center-of-mass (c.m.) energy using the vertex position determined by the TPC and the projected trajectory of the ions entering the target. In the range of 500–1000 keV the FWHM energy resolution and the add-back photopeak efficiency of the DALI2$^+$ array were 13.5% (500 keV)–10.8% (1000 keV) and 45% (500 keV)–30% (1000 keV), respectively. Further details of the DALI2$^+$ setup, the Doppler correction, the add-back procedure as well as the MINOS device, and the track reconstruction can be found in the previous papers on this experiment [20,22,24–31] and elsewhere [35–37].

A. ^{61}V

Most of the events belonging to fragment ^{61}V and associated with γ rays came from the (p, pn) reaction contaminated with events from the ^{62}V(p, p') ^{62}V$^* \rightarrow$ ^{61}V$^* + n$ decay channel (upper panel of Fig. 1). As discussed in our earlier papers [42,43], this Doppler-corrected singles γ-ray spectrum contains a two-component background: a low-energy part (<500 keV) originating from atomic processes and a high-energy part coming from other sources, mainly the reactions of the scattered particles on the materials surrounding the target. This background was successfully modeled by a double-exponential function with four free parameters for other reactions of this experiment [20,24,26,27,29] as well as for our earlier similar experiments [18,43–49].

Two distinct peaks are visible in the spectrum at around 650 and 800 keV and a structure of peaks between 900 and 1300 keV. In order to determine the statistical confidence, the energy, and the intensity of these peaks a simulation was performed by a GEANT4 [50] application [51]. This application could provide the response function of the DALI2$^+$ setup for a γ ray emitted by the fast-moving projectile taking into account the intrinsic experimental resolution of the NaI(Tl) detectors. The resulting response functions were added together with individual scaling parameters plus the double-exponential function to fit the spectrum using the likelihood method [52] of the ROOT framework [53], which gave reliable results for the spectra with low statistics [24,54]. The total fit with a reduced χ^2 (χ^2_ν) of 1.50 is presented by a red line while the background is plotted by a blue line. This analysis showed that the 900–1300-keV peak structure could be fitted with two peaks at 978(20) and 1106(18) keV, and the locations of the lower-energy peaks were determined at 643(6) and 823(8) keV. The statistical confidence of all the peaks reached the 3σ limit of unambiguous existence: 6.7σ (643), 7.8σ (823), 4.5σ (978), 7.6σ (1106). The stability of the statistical significance of the peaks was also checked using larger bin sizes of 25 and 40 keV, and only a small change
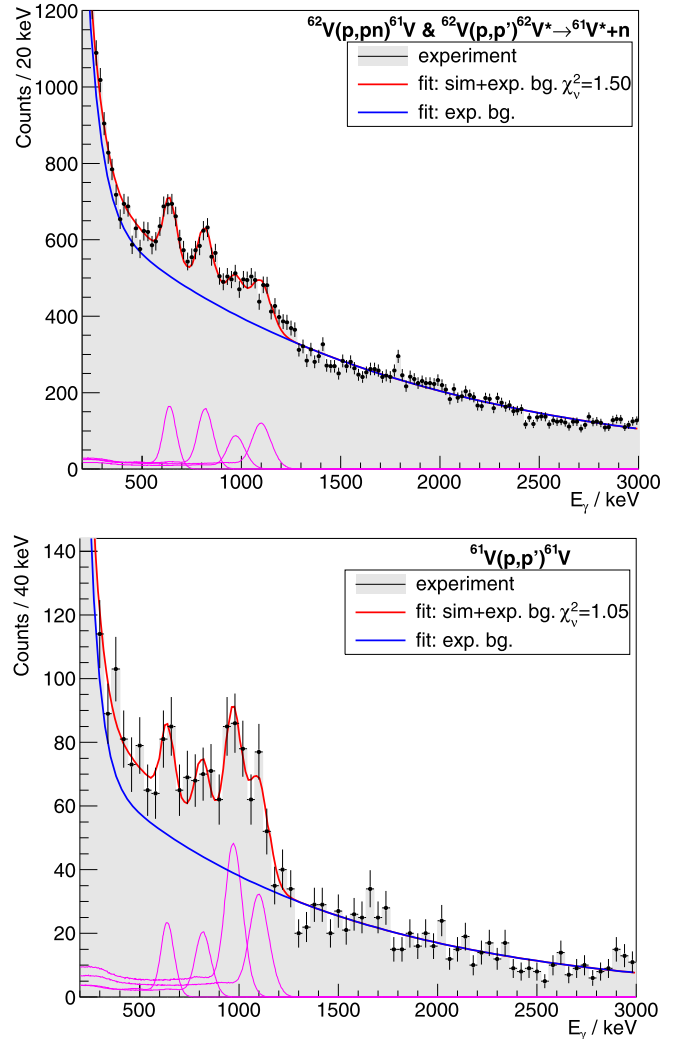

FIG. 1. Doppler corrected singles γ-ray spectra for ^{61}V using vertex reconstruction and add-back procedure [upper panel: Mainly ^{62}V(p, pn) ^{61}V reaction including ^{62}V(p, p') ^{62}V$^* \rightarrow$ ^{61}V$^* + n$ decay channel; lower panel: Inelastic scattering]. The data with error bars and shaded area represent the experimental spectrum, the red line is the simulation plus a free-parameter double-exponential background, and the latter function (exponential background) is also plotted separately as a blue line. The magenta lines illustrate the individual response functions for the transitions.

($<0.2\sigma$) was observed. On one hand, the quoted uncertainties for the energy of the γ rays originated from the statistics, the energy calibration (5 keV), and the background estimation. Furthermore, the transitions may be associated with half-lives. For the response of the DALI2$^+$ setup, this could result in shifted peak energies and increased peak widths (for short half-lives of about some 10 ps) or asymmetric, distorted peaks with long, low-energy tails (for half-lives above about 100 ps). The 643 and the 823-keV transitions did not show any sign of low-energy tails, which is obviously due to their short half-lives. For the 978- and 1106-keV transitions even a single-particle $E2$ character would bring half-lives of 42 and 23 ps, respectively. Therefore, only a little width increase (few keV) and an energy shift (<10 keV) of the peaks needed to

be considered for all the transitions detected. The systematic uncertainties on the peak energies coming from the analysis of these unknown half-lives were quadratically added to the uncertainties listed above.

Although the inelastic scattering was not as strong as the (p, pn) channel it could also be studied. The corresponding Doppler-corrected singles γ-ray spectrum is presented in the lower panel of Fig. 1. The fitting was performed including the fixed location of the four peaks determined for the (p, pn) case, and an excellent fit with $\chi_\nu^2 = 1.05$ was obtained.

Based on the observed number of γ rays, the efficiency of the DALI2$^+$ setup and that of the MINOS device, and also the number of the incoming ions taking into account the effective transmission of 51% for ^{61}V and of 49% for ^{59}V through the SAMURAI spectrometer (including the efficiency of the beam-line detectors, the beam losses in the detectors and the target), the γ-ray-production cross sections of $\sigma(ppn; 643\gamma) = 1.05(14)$ mb, $\sigma(ppn; 823\gamma) = 1.26(16)$ mb, $\sigma(ppn; 978\gamma) = 0.69(16)$ mb, $\sigma(ppn; 1106\gamma) = 1.41(18)$ mb associated with the transitions in the (p, pn) channel and the γ-ray-production cross sections of $\sigma(pp'; 643\gamma) = 0.09(3)$ mb, $\sigma(pp'; 823\gamma) = 0.11(4)$ mb, $\sigma(pp'; 978\gamma) = 0.31(5)$ mb, $\sigma(pp'; 1106\gamma) = 0.24(5)$ mb for the inelastic scattering were determined. Further details on the determination of the effective transmission can be found elsewhere [54]. Since the γ-ray spectrum in the upper panel of Fig. 1 included events related to the neutron-unbound states of ^{62}V inelastically excited in the target and decaying to the excited states of ^{61}V, a subtraction of this contribution to the cross sections was performed. For this purpose, the relative energy (E_{rel}) of the ^{61}V +neutron system was reconstructed. This energy is simply the difference between the invariant mass before and after the decay, so it shows the excited states above the neutron separation energy S_n of ^{62}V. For the reconstruction, the momentum of the ^{61}V ions were determined by the SAMURAI spectrometer and the momentum of the neutron by the NEBULA + NeuLAND TOF spectrometer. The TOF calibration was performed using the γ-ray flash arriving at the spectrometer from the target before the neutrons. The resulting E_{rel} spectrum was corrected for the neutron detection efficiency of the NEBULA + NeuLAND setup (55% at 100 keV, 20% at 5 MeV) determined by GEANT4 simulations. The Doppler-corrected γ-ray spectrum of ^{61}V contaminating the (p, pn) channel was prepared by gating on the efficiency-corrected E_{rel} spectrum of ^{62}V between 0 and 5000 keV covering $S_n \leqslant 5$ MeV. This γ-ray spectrum of ^{61}V was analyzed in the same manner as the nonsubtracted γ-ray spectrum using the fixed location of the peaks determined earlier. The contribution was found to vary between 10% and 30% depending on the different transitions and subtracted from the cross sections. In the end the uncertainties of the final cross sections listed above are dominated by the statistical uncertainty originating from the fits but they also include quadratically the other contributions coming from the choice of the background, the simulated photopeak efficiency of the DALI2$^+$ array, the target thickness, and the subtraction. The inclusive cross section for the ^{62}V(p, pn)^{61}V + ^{62}V(p, p')^{62}V$^* \rightarrow$ ^{61}V $+n$ channels was extracted to be 62(3) mb.
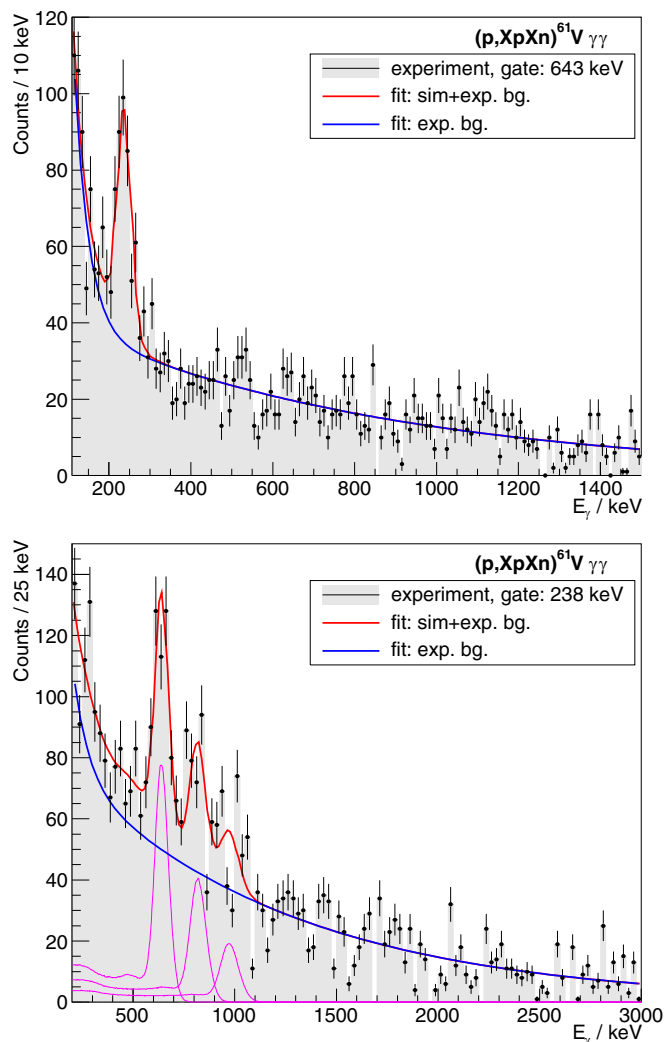

FIG. 2. Doppler corrected coincidence γ-ray spectra for ^{61}V using all the reaction channels. The data with error bars and shaded area represent the experimental spectrum, the red line is the simulation plus a free-parameter double-exponential background, and the latter function (exponential background) is also plotted separately as a blue line. The magenta lines illustrate the individual response functions for the transitions. Upper panel: Events coincident with the 643-keV transition (gate: 590–690 keV) with the subtraction of background events using a side gate between 1300 and 1400 keV; lower panel: Events coincident with the 238-keV transition (gate: 190–290 keV) with the subtraction of background events using a side gate between 690 and 790 keV.

The statistics allowed us to prepare a $\gamma\gamma$ matrix of the events in order to uncover the coincidences between the γ rays. The upper panel of Fig. 2 shows the Doppler-corrected γ-ray spectrum in coincidence with the 643-keV transition, the strongest one in the singles spectrum. The gate for the 643-keV transition was put between 590 and 690 keV, and the background events with a gate between 1300 and 1400 keV just above the energy of the detected peaks were subtracted from the coincidence spectrum. Owing to the reduction of the background in the coincidence spectrum, a strong peak was revealed at an energy of 238(4) keV by the fitting procedure
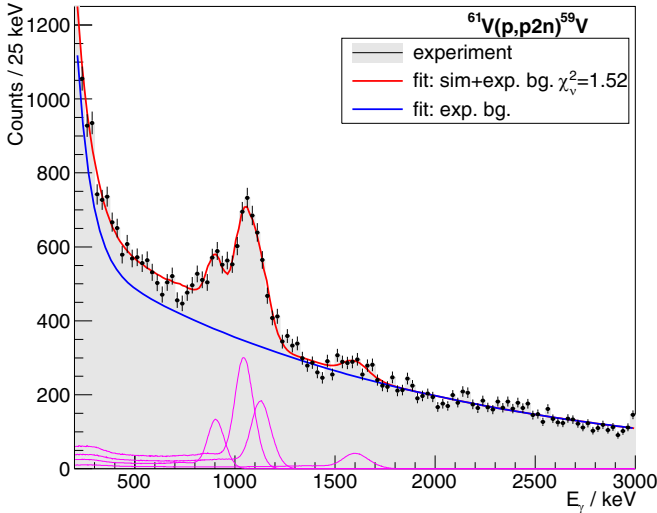
FIG. 3. Doppler-corrected singles γ-ray spectra for ^{59}V originating from the $(p, p2n)$ reaction channel using vertex reconstruction and add-back procedure. The data with error bars and shaded area represent the experimental spectrum, the red line is the simulation plus a free-parameter double-exponential background, and the latter function (exponential background) is also plotted separately as a blue line. The magenta lines illustrate the individual response functions for the transitions.

described for the (p, pn) reaction channel analysis. By putting a gate on this 238-keV transition (gate: 190–290 keV), and again subtracting the background events with a gate right above the 238-keV peak between 290 and 390 keV, we ended up with the spectrum in the lower panel of Fig. 2 which, was fitted using the fixed location of the four peaks determined in the (p, pn) reaction channel. The spectrum clearly establishes the 238-643 and the 238-823 coincidences while it also indicates the 238-978 coincidence. No further coincidences were found between the detected transitions.

B. ^{59}V

The only reaction channel that could be analyzed for ^{59}V is the $(p, p2n)$ one, for which the Doppler-corrected singles γ-ray spectrum is shown in Fig. 3. This spectrum includes a structure of peaks in the energy range of 700–1300 keV, and a small peak at around 1600 keV. An analysis similar to that of the ^{62}V(p, pn) ^{61}V reaction channel resolved three transitions at energies of 910(11), 1051(13), and 1135(23) keV for the structure of peaks while the high-energy peak was determined at 1611(24) keV. The statistical confidences of the peaks were derived to be 6.1σ (910), 16.4σ (1051), 10.5σ (1135), and 4.0σ (1611), and again changed little ($<0.2\sigma$) by applying different bin sizes. Since the energies of the peaks were very close to each other the $\gamma\gamma$ matrix of the events did not give any conclusive suggestion about the coincidences between the transitions.

IV. INTERPRETATION OF THE EXPERIMENTAL DATA

For the interpretation of the observed data, the low-energy level and decay scheme of ^{59}V and ^{61}V as well as the spec-

troscopic factors for the (p, pn) reaction were calculated by large-scale shell-model calculations. The distorted wave impulse approximation (DWIA) framework was also applied to provide the single-particle cross sections in order to assist the explanation of the experimental results. The inelastic scattering cross sections were determined by a coupled-channels calculation in order to derive information on the deformation of the nuclei in question. Similar analyses on odd-A isotopes were performed in the past (e,g, for ^{31}Na [55], ^{33}Mg [56], ^{43}Ar [57], ^{49,51}Ca [58]), and the deformations were found to be reasonable compared to the neighboring even-even isotopes.

All these theoretical approaches were exactly the same as those we used in our previous publication [22], in which they were thoroughly discussed, therefore only some fundamental parts are repeated now. The shell-model calculation was performed with the code ANTOINE [59,60], and the Hamiltonian based on the LNPS [8] interaction. For the $M1/E2$ reduced transition probabilities, effective charges $e_p = 1.31$, $e_n = 0.46$ for $B(E2)$ and $g_l^n = 0.0$, $g_s^n = -2.87$, $g_l^p = 1.0$, $g_s^p = 4.19$ for the $B(M1)$ values [60,61] were taken because the standard effective charges ($e_p = 1.5$, $e_n = 0.5$) overestimated the $B(E2)$ values for neutron-rich chromium and iron isotopes [62]. On the other hand, the reduced effective charges, derived in perturbation theory in Ref. [61], proved to be successful in interpreting the experimental results near the $N = 40$ shell gap [13,15,18–20,43,63–65]. The details of the DWIA approach can be found in an earlier publication [66]. The coupled-channels calculation was realized by the ECIS code [67] using the symmetric rotational model. The optical potential parameters were taken from the global phenomenological set of Koning and Delaroche [68], which was successfully used in similar experiments [43]. As a usual approach, the quadrupole matter (δ_2^M) and Coulomb deformation lengths (δ_2^C), the model parameters were kept equal because the proton and neutron distributions do not differ significantly for a wide range of nuclei [69–71].

A. ^{61}V

The partial level and decay scheme from the shell model is presented on the left-hand side of Fig. 4. The ground state is calculated to be $3/2^-$, which is consistent with the β-decay [72] and knockout data [19]. Thus, the $3/2^-$ spin-parity assignment to the ground state is a realistic starting point for the interpretation of the experimental results.

Since the (p, p') reaction usually populates the lowest-energy levels strongly coupled to the ground state, the lowest few excited states (which are the first calculated levels for each spin up to 11/2) are shown in Fig. 4.

^{61}V lies on the $N = 38$ isotonic chain between ^{62}Cr and ^{60}Ti. The low-energy level structures of both neighboring nuclei were successfully described by the shell model with the LNPS interaction [19,73] as well as the $B(E2; 0_1^+ \rightarrow 2_1^+)$ value of ^{62}Cr [62,73], and a large quadrupole deformation parameter of around $\beta_2 = 0.3$ was derived for ^{62}Cr while LNPS also suggested a β_2 value around 0.2 for ^{60}Ti. Using this lower $\beta_2 = 0.2$ value, our coupled-channels calculation gives (p, p') excitation cross sections of 2.5 and 1.5 mb for the calculated $5/2_1^-$ and the $7/2_1^-$ levels, respectively. These calculated cross
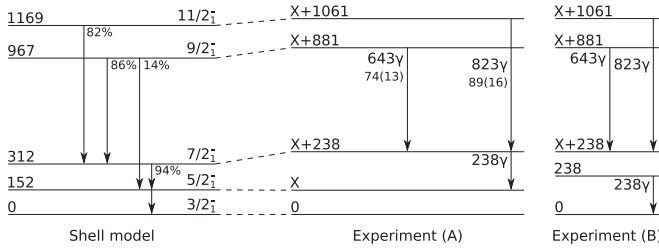
FIG. 4. Partial level and decay scheme of ^{61}V. Three of the five observed γ rays could be placed in two slightly different ways (Experiments A and B). X is the energy of a transition (<200 keV) not detected in the present experiment. The origin of the remaining two γ rays (978, 1106) could not be unambiguously determined; they probably belong to the decay of states above the $11/2_1^-$ level. The intensity of the two γ rays relative to the 1106-keV transition found in the singles spectrum of the (p, pn) channel is also indicated next to the downward arrows. The experimental data were compared with our shell-model calculations on the left-hand side where the calculated γ-ray branching ratios are also written next to the downward arrows.

sections are about an order of magnitude larger than the observed $\sigma(pp'; 643\gamma) = 0.09(3)$ mb, $\sigma(pp'; 823\gamma) = 0.11(4)$ mb, $\sigma(pp'; 978\gamma) = 0.31(5)$ mb, $\sigma(pp'; 1106\gamma) = 0.24(5)$ mb values. For the coupled-channels calculation, the simplest assumption of a $K = 3/2$ band was assumed, and the level structure with spin-parities from the shell model in Fig. 4 was used. The uncertainty in the cross sections due to the change of optical model parameters as the beam energy decreases in the target was found to be negligible, therefore the mean beam energy in the target was chosen for the optical model parameters. It is also worth mentioning that the calculated cross sections negligibly depend on the energy of the levels in this low-energy regime. Therefore, we conclude that the γ rays observed in the (p, p') reaction cannot be associated with the transitions from the $5/2_1^-$ and the $7/2_1^-$ levels, which is also supported by the large energy difference between the expected γ rays of around 150 keV (emitted by the deexciting $5/2_1^-$ and the $7/2_1^-$ levels) and the experimental ones. Similar cross-section arguments hold for higher-lying levels with spin $J \leqslant 7/2$ due to $J_{gs}(^{61}V) = 3/2$.

However, the theoretical $9/2_1^-$ and $11/2_1^-$ levels seem to be very good candidates for the assignment of two of the γ rays observed (643, 823) in the (p, p') reaction. Both of them predominantly decay to the $7/2_1^-$ level with transition energies of 655 and 857 keV, which are close to the experimental values. Also, due to their spin-parity they are expected to be weakly excited in the (p, p') reaction, which is also in line with the observation. The experimental production cross sections of the 643-and 823-keV γ rays are similar, thus both can be assigned either to the $9/2_1^-$ level or the $11/2_1^-$ level because they are close to each other in energy. From the coincidence spectra, it was learned that both γ ray transitions were in coincidence with the 238-keV γ ray. Therefore, it is a natural assumption that this γ ray belongs to the transition either between the theoretical $7/2_1^-$ and $5/2_1^-$ levels or the $5/2_1^-$ and $3/2_1^-$ levels. This implies the low-energy level schemes (Experiments A and B) shown in Fig. 4, where X is the energy of a transition lower than 200 keV unobserved due to the intense

background in this energy regime, and the excitation cross sections are $\sigma_{\exp}(pp'; X + 881) = 0.10(3)$ mb, $\sigma_{\exp}(pp'; X + 1061) = 0.13(5)$ mb, $\sigma_{\exp}(ppn; X + 881) = 1.22(15)$ mb, $\sigma_{\exp}(ppn; X + 1061) = 1.54(18)$ mb taking into account the calculated γ-ray branching ratios of the $9/2_1^-$ (86%) and the $11/2_1^-$ (82%) levels. It is important to emphasize that no feeding was taken into account to the 881-keV and the 1061-keV levels since neither the 978-keV transition nor the 1106-keV transition were found to be in coincidence with the 643- and the 823-keV transitions depopulating the $X + 881-$ and the $X + 1061$-keV levels, respectively.

Following the train of thought in our previous paper on ^{63}V [22], the coupled-channels calculation was performed. This analysis implied multistep excitations of the $9/2_1^-$ and $11/2_1^-$ states through the $5/2_1^-$ and $7/2_1^-$ states which was taken into account by the quadrupole deformation length parameter (δ_2). Additionally, single-step excitations could also occur in the inelastic scattering reducing δ_2, and could be handled by the hexadecapole deformation length parameter (δ_4). Three scenarios were investigated: (1) $\delta_4 = 0$; (2) $\delta_4/\delta_2 = 1/3$ which was the upper limit experimentally determined for the island-of-inversion nucleus ^{32}Mg [74] around $N = 20$; (3) $\delta_4/\delta_2 = 0.6$ which is a typical value for the island-of-inversion nuclei around $N = 40$ taken from a recent theoretical work on the importance of hexadecapole deformation in this region [75] using Skyrme interaction SkM* best reflecting the available experimental data. These cases resulted in the following values reproducing the (p, p') excitation cross sections of $\sigma_{\exp}(pp'; X + 881) = 0.10(3)$ mb and $\sigma_{\exp}(pp'; X + 1061) = 0.13(5)$ mb taking into account the calculated γ-ray branching ratios of the $9/2_1^-$ (86%) and the $11/2_1^-$ (82%) levels: (1) $\delta_2 = 1.75(20)$ fm [$\beta_2 = 0.37(4)$]; (2) $\delta_2 = 0.75(6)$ fm [$\beta_2 = 0.16(1)$] and $\delta_4 = 0.25(2)$ fm [$\beta_4 = 0.05(1)$], and (3) $\delta_2 = 0.45(5)$ fm [$\beta_2 = 0.10(1)$] and $\delta_4 = 0.27(2)$ fm [$\beta_4 = 0.06(1)$]. The quadrupole (β_2) and hexadecapole (β_4) deformation parameters were calculated with the well-known relation $\delta_i = \beta_i \times 1.2$ fm $\times A^{1/3}$. The quoted uncertainty originates from the uncertainty of the observed cross-section. However, it is worth noting that the choice of the optical potential usually adds about 10% uncertainty to the deformation parameter [43,76]. Our shell-model calculation gives $\beta_2^{\text{theor}} = 0.30$, between the experimental values for scenarios (1) and (2). The large β_2 value of scenario (1) would place ^{61}V in the island of inversion, which is suggested by our shell-model calculation as well as the Skyrme-HF calculation [75]; however, the latter would also require a large β_4 value in contrast to the assumption for scenario (1). Scenarios (2) and (3) used δ_4/δ_2 values suggested for the island-of-inversion nuclei experimentally and theoretically, nevertheless the derived small β_2 values would indicate that ^{61}V is outside of the island of inversion. The remaining two experimental γ rays (978, 1106 keV) did not show clear coincidence with the other observed transitions, and their production cross section was low (<0.36 mb), therefore, they probably arise from the many calculated levels (approximately 150 up to the expected neutron separation energy of 5160(300) keV [77]; see Table I for the most important ones) above the $11/2_1^-$ one, which decay to the ground state via transitions not observed (except for 978 and 1106 keV) in the present experiment.

TABLE I. Theoretical level energies (E_theor), cross sections for the reaction $^{62}\text{V}(p, pn)\,^{61}\text{V}(\sigma_\text{theor})$ up to the expected neutron separation energy of 5.160(300) MeV [77]. The level energies and the spectroscopic factors originate from our shell-model calculations with $J^\pi(^{62}\text{V}) = 3^+$ or $J^\pi(^{62}\text{V}) = 1^+$ while the cross sections are obtained by combining the DWIA cross sections and the spectroscopic factors. The uncertainty in the DWIA framework and its input is about 20%, as discussed in Ref. [66]. Only those excited states are shown for which the theoretical spectroscopic factors exceeds 0.1.

E_theor(MeV)	J^π	$J^\pi(^{62}\text{V})$	σ_theor(mb)
0	$3/2^-$	$3^+, 1^+$	1.0–1.7
0.152	$5/2^-$	$3^+, 1^+$	1.2–2.1
0.312	$7/2^-$	$3^+, 1^+$	0.3–0.5
0.967	$9/2^-$	3^+	0.5–0.9
1.169	$11/2^-$	3^+	0.5–0.8
2.171	$3/2^+$	$3^+, 1^+$	0.8–1.3
2.251	$5/2^+$	3^+	0.8–1.3
2.310	$7/2^+$	$3^+, 1^+$	0.6–1.0
2.492	$9/2^+$	3^+	0.4–0.7
2.541	$3/2^-$	1^+	0.4–0.6
2.577	$11/2^+$	$3^+, 1^+$	0.9–1.4
2.706	$11/2^+$	1^+	0.4–0.7
2.939	$11/2^+$	1^+	0.6–0.9
3.031	$15/2^+$	3^+	2.1–3.3
3.830	$3/2^-$	1^+	0.6–0.8
3.834	$11/2^-$	3^+	0.4–0.6
4.014	$3/2^-$	1^+	2.2–3.3
4.039	$7/2^-$	$3^+, 1^+$	0.4–0.6
4.074	$7/2^-$	3^+	0.6–0.9
4.139	$3/2^-$	1^+	0.3–0.5
4.139	$5/2^-$	1^+	1.8–2.7
4.269	$7/2^-$	1^+	0.4–0.6
4.287	$3/2^-$	1^+	0.5–0.8
4.369	$9/2^-$	3^+	0.4–0.6
4.387	$5/2^-$	1^+	0.7–1.0
4.441	$7/2^-$	3^+	1.1–1.5
4.534	$7/2^-$	1^+	0.3–0.5
4.586	$3/2^-$	1^+	0.4–0.6
4.659	$5/2^-$	3^+	0.5–0.7
4.686	$7/2^-$	3^+	0.7–1.1
4.712	$9/2^-$	3^+	0.9–1.3
4.723	$11/2^-$	3^+	0.4–0.6
4.839	$5/2^-$	3^+	0.3–0.5
4.999	$9/2^-$	3^+	0.5–0.7

Regarding the (p, pn) channel, unfortunately little is known about the seed nucleus ^{62}V. The spin-parity of its ground state is expected to be 3^+ based on systematics [78]; however, a low-lying isomer state with long lifetime (in the ms range) and with $J^\pi = 1^+$ likely exist also in this nucleus as it was discovered in ^{60}V [79]. This means that when discussing the population of states in ^{61}V by the (p, pn) reaction both possibilities for the ground state of ^{62}V should be taken into account. Therefore, a precise comparison of the theoretical and experimental cross sections is not straightforward; however, a qualitative analysis of the experimental data could still be performed. Table I lists the level energy (E_theor), the spin-parity (J^π), and the estimated cross section for the re-

action $^{62}\text{V}(p, pn)\,^{61}\text{V}$ (σ_theor) of those 29 levels for which the spectroscopic factor was calculated to be larger than 0.1 with $J^\pi(^{62}\text{V}) = 3^+$ or $J^\pi(^{62}\text{V}) = 1^+$ assumption up to the expected neutron separation energy. DWIA calculation gives single-particle cross sections averaged for the beam energy in the middle of target between 3.2 and 7.4 mb depending on the single-particle state taken into account. Using these values and assuming the assignment from the analysis of the (p, p') reaction, we end up with theoretical (p, pn) cross sections of $\sigma_\text{theor}(ppn; 9/2_1^-) = 0.5$–0.9 mb and $\sigma_\text{theor}(ppn; 11/2_1^-) = 0.5$–0.8 mb (see Table I). These cross-section values are close to the experimental ones of $\sigma_\text{exp}(ppn; X + 881) = 1.22(15)$ mb, $\sigma_\text{exp}(ppn; X + 1061) = 1.54(18)$ mb. Since the $9/2_1^-$ and $11/2_1^-$ levels are not expected to be populated by the (p, pn) reaction according to the shell model using $J_{gs}^\pi(^{62}\text{V}) = 1^+$, our results indicate either 3^+ for the ground state of ^{62}V or significant production of a possible 3^+ isomeric state in ^{62}V. The appearance of the other two experimental transitions (978, 1106) in the (p, pn) channel is consistent with the suggestion from the (p, p') data, i.e., they probably originate from the decay of the states lying higher than the $11/2_1^-$ associated with significant (>0.1) spectroscopic factors.

Summing the individual theoretical cross-sections in Table I for the (p, pn) reaction, we end up with a value of 24 or 37 mb depending on whether the minimum or the maximum values are used. The nonlisted states add an extra ≈ 10 mb to the summed minimum and maximum values of this cross section, resulting in an average value of ≈ 41 mb. The contribution to the experimental inclusive cross section of 62(3) mb coming from the unbound states of ^{62}V populated by the (p, p') reaction and decaying to the excited states of ^{61}V was determined to be 20%. Subtracting this value, we arrive at around 50 mb, which is not far from the theoretical average value of 41 mb. Since the subtracted experimental value (50 mb) still contains the decay of the unbound states in ^{62}V to the ground state of ^{61}V, expected to be large compared to the decay to the excited states of ^{61}V, this is likely one of largest source of the remaining difference between the theoretical and the experimental cross sections. Furthermore, it is also noted that LNPS interactions works with a ^{48}Ca core, so a possible small contribution from the $\nu f_{7/2}$ orbit is not included in the calculation.

B. ^{59}V

Since we can rely only on the singles γ-ray spectrum in the $(p, p2n)$ reaction channel for ^{59}V, the placements of the observed γ rays are tentative and basically based on the comparison to the shell-model level scheme and the calculated branching ratios as well as the resemblance to the ^{61}V and ^{63}V isotopes. Looking at the partial level and decay scheme of ^{59}V in Fig. 5, there are three calculated low-lying states with spin-parities $5/2_1^-, 3/2_1^-, 7/2_1^-$ with energies too small to associate the observed transitions to their decay. The most probable assignment of the experimental γ rays is again connected to the theoretical $9/2_1^-$ and the $11/2_1^-$ levels in analogy with ^{61}V and ^{63}V. According to the shell model calculation the $11/2_1^-$ level exclusively decay to the ground state with a single transition while two γ rays are expected
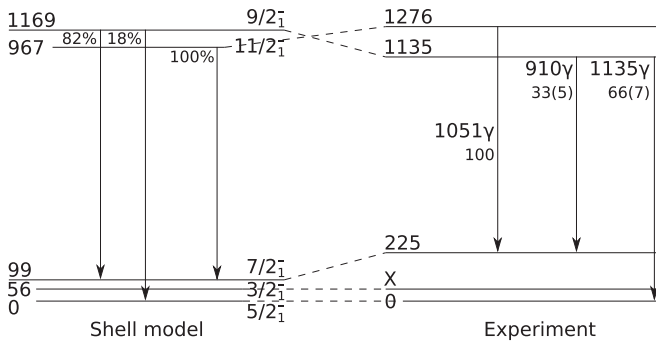
FIG. 5. Partial level and decay scheme of ^{59}V. Three of the four observed γ rays could be placed in the level scheme (Experiment) using the analogy to ^{59}V and ^{61}V as well as our shell-model calculations on the left-hand side. X is the energy of a transition (<200 keV) not detected in the present experiment. The origin of the remaining γ ray (1611) could not be unambiguously determined; it probably belongs to the decay of states above the $11/2_1^-$ level. The relative intensity of the three γ rays found in the singles spectrum of the $(p, p2n)$ channel is also indicated next to the downward arrows while the calculated γ-ray branching ratios are also written next to the downward arrows for the shell model.

to be emitted during the decay of the $9/2^-$ level. Based on the experimentally determined relative γ-ray intensities, the most plausible placement of three of the detected transitions is plotted on the right side of Fig. 5. The remaining experimental γ ray (1611) probably again arises from the decay of a state above the $11/2_1^-$ level.

V. SUMMARY

The low-lying excited states of ^{59}V and ^{61}V were studied for the first time by proton inelastic scattering (for ^{61}V) and the neutron knockout reaction (for both ^{59}V and ^{61}V). Five transitions were observed for ^{61}V, and four γ rays were detected for ^{59}V. For each nucleus three of these transitions were associated to the decay of the theoretical levels determined by our shell model. Analyzing the excitation cross section of the two excited states for ^{61}V in the (p, p') reaction, the quadrupole and hexadecapole deformation parameters were extracted in three scenarios. Comparing the derived values to the theoretical calculations it was not possible to unambiguously determine whether ^{61}V belongs to the *island of inversion* due to the role of the hexadecapole deformation. This calls

for more detailed experimental studies of the hexadecapole deformation of the nuclei around the island of inversion in order to find its boundaries.

[1] C. Thibault, R. Klapisch, C. Rigaud, A. M. Poskanzer, R. Prieels, L. Lessard, and W. Reisdorf, Phys. Rev. C **12**, 644 (1975).

[2] G. Huber, F. Touchard, S. Büttgenbach, C. Thibault, R. Klapisch, H. T. Duong, S. Liberman, J. Pinard, J. L. Vialle, P. Juncar *et al.*, Phys. Rev. C **18**, 2342 (1978).

[3] C. Détraz, D. Guillemaud, G. Huber, R. Klapisch, M. Langevin, F. Naulin, C. Thibault, L. C. Carraz, and F. Touchard, Phys. Rev. C **19**, 164 (1979).

[4] E. K. Warburton, J. A. Becker, and B. A. Brown, Phys. Rev. C **41**, 1147 (1990).

[5] Y. Utsuno, T. Otsuka, T. Mizusaki, and M. Honma, Phys. Rev. C **60**, 054315 (1999).

[6] T. Otsuka, A. Gade, O. Sorlin, T. Suzuki, and Y. Utsuno, Rev. Mod. Phys. **92**, 015002 (2020).

[7] M. Hannawald, T. Kautzsch, A. Wöhr, W. B. Walters, K.-L. Kratz, V. N. Fedoseyev, V. I. Mishin, W. Böhmer, B. Pfeiffer, V. Sebastian *et al.*, Phys. Rev. Lett. **82**, 1391 (1999).

[8] S. M. Lenzi, F. Nowacki, A. Poves, and K. Sieja, Phys. Rev. C **82**, 054301 (2010).

[9] F. Recchia, S. M. Lenzi, S. Lunardi, E. Farnea, A. Gadea, N. Mărginean, D. R. Napoli, F. Nowacki, A. Poves, J. J. Valiente-Dobón *et al.*, Phys. Rev. C **85**, 064305 (2012).

[10] L. Canete, S. Giraud, A. Kankainen, B. Bastin, F. Nowacki, A. Poves, P. Ascher, T. Eronen, V. Alcindor, A. Jokinen, A. Khanam, I.D. Moore, D.A. Nesterenko, F. De Oliveira Santos, H. Penttila, C. Petrone, I. Pohjalainen, A. de Roubin, V.A. Rubchenya, M. Vilen, J. Aysto, Phys. Rev. C **101**, 041304(R) (2020).

[11] J. Ljungvall, A. Gorgen, A. Obertelli, W. Korten, E. Clement, G. deFrance, A. Burger, J.P. Delaroche, A. Dewald, A. Gadea, L. Gaudefroy, M. Girod, M. Hackstein, J. Libert, D. Mengoni, F. Nowacki, T. Pissulla, A. Poves, F. Recchia, M. Rejmund, W. Rother, E. Sahin, C. Schmitt, A. Shrivastava, K. Sieja, J.J. Valiente-Dobon, K.O. Zell, M. Zielinska, Phys. Rev. C **81**, 061301(R) (2010).

[12] S. Naimi, G. Audi, D. Beck, K. Blaum, C. Böhm, C. Borgmann, M. Breitenfeldt, S. George, F. Herfurth, A. Herlert *et al.*, Phys. Rev. C **86**, 014325 (2012).

[13] H. L. Crawford, R. M. Clark, P. Fallon, A. O. Macchiavelli, T. Baugher, D. Bazin, C. W. Beausang, J. S. Berryman, D. L. Bleuel, C. M. Campbell *et al.*, Phys. Rev. Lett. **110**, 242701 (2013).

[14] S.N. Liddick, S. Suchyta, B. Abromeit, A. Ayres, A. Bey, C.R. Bingham, M. Bolla, M.P. Carpenter, L. Cartegni, C.J. Chiara, H.L. Crawford, I.G. Darby, R. Grzywacz, G. Gurdal, S. Ilyushkin, N. Larson, M. Madurga, E.A. McCutchan, D. Miller, S. Padgett, S.V. Paulauskas, J. Pereira, M.M. Rajabali, K. Rykaczewski, S. Vinnikova, W.B. Walters, S. Zhu, Phys. Rev. C **84**, 061305(R) (2011).

[15] X. Liu, Z. Liu, B. Ding, P. Doornenbal, A. Obertelli, S. Lenzi, P. Walker, L. Chung, B. Linh, G. Authelet *et al.*, Phys. Lett. B **784**, 392 (2018).

[16] A. Gade, A. Gade, R.V.F. Janssens, T. Baugher, D. Bazin, B.A. Brown, M.P. Carpenter, C.J. Chiara, A.N. Deacon, S.J. Freeman, G.F. Grinyer, C.R. Hoffman, B.P. Kay, F.G. Kondev, T. Lauritsen, S. McDaniel, K. Meierbachtol, A. Ratkiewicz, S.R. Stroberg, K.A. Walsh, D. Weisshaar, R. Winkler, S. Zhu, Phys. Rev. C **81**, 051304(R) (2010).

[17] S. Suchyta, S. N. Liddick, C. J. Chiara, W. B. Walters, M. P. Carpenter, H. L. Crawford, G. F. Grinyer, G. Gürdal, A. Klose, E. A. McCutchan *et al.*, Phys. Rev. C **89**, 067303 (2014).

[18] C. Santamaria, C. Louchart, A. Obertelli, V. Werner, P. Doornenbal, F. Nowacki, G. Authelet, H. Baba, D. Calvet, F. Château *et al.*, Phys. Rev. Lett. **115**, 192501 (2015).

[19] A. Gade, R. V. F. Janssens, D. Weisshaar, B. A. Brown, E. Lunderberg, M. Albers, V. M. Bader, T. Baugher, D. Bazin, J. S. Berryman *et al.*, Phys. Rev. Lett. **112**, 112503 (2014).

[20] M. Cortés, W. Rodriguez, P. Doornenbal, A. Obertelli, J. Holt, S. Lenzi, J. Menéndez, F. Nowacki, K. Ogata, A. Poves *et al.*, Phys. Lett. B **800**, 135071 (2020).

[21] S. Michimasa, M. Kobayashi, Y. Kiyokawa, S. Ota, R. Yokoyama, D. Nishimura, D. S. Ahn, H. Baba, G. P. A. Berg, M. Dozono *et al.*, Phys. Rev. Lett. **125**, 122501 (2020).

[22] M. M. Juhász, Z. Elekes, D. Sohler, K. Sieja, K. Yoshida, K. Ogata, P. Doornenbal, A. Obertelli, H. Baba, F. Browne *et al.*, Phys. Rev. C **103**, 064308 (2021).

[23] B. Pritychenko, M. Birch, B. Singh, and M. Horoi, At. Data Nucl. Data Tables **107**, 1 (2016).

[24] H. N. Liu, A. Obertelli, P. Doornenbal, C. A. Bertulani, G. Hagen, J. D. Holt, G. R. Jansen, T. D. Morris, A. Schwenk, R. Stroberg *et al.*, Phys. Rev. Lett. **122**, 072502 (2019).

[25] S. Chen, J. Lee, P. Doornenbal, A. Obertelli, C. Barbieri, Y. Chazono, P. Navrátil, K. Ogata, T. Otsuka, F. Raimondi *et al.*, Phys. Rev. Lett. **123**, 142501 (2019).

[26] Y. Sun, A. Obertelli, P. Doornenbal, C. Barbieri, Y. Chazono, T. Duguet, H. Liu, P. Navrátil, F. Nowacki, K. Ogata *et al.*, Phys. Lett. B **802**, 135215 (2020).

[27] M. L. Cortés, W. Rodriguez, P. Doornenbal, A. Obertelli, J. D. Holt, J. Menéndez, K. Ogata, A. Schwenk, N. Shimizu, J. Simonis *et al.*, Phys. Rev. C **102**, 064320 (2020).

[28] B. D. Linh, A. Corsi, A. Gillibert, A. Obertelli, P. Doornenbal, C. Barbieri, S. Chen, L. X. Chung, T. Duguet, M. Gómez-Ramos *et al.*, Phys. Rev. C **104**, 044331 (2021).

[29] M. Juhász, Z. Elekes, D. Sohler, Y. Utsuno, K. Yoshida, T. Otsuka, K. Ogata, P. Doornenbal, A. Obertelli, H. Baba *et al.*, Phys. Lett. B **814**, 136108 (2021).

[30] F. Browne, S. Chen, P. Doornenbal, A. Obertelli, K. Ogata, Y. Utsuno, K. Yoshida, N. L. Achouri, H. Baba, D. Calvet *et al.*, Phys. Rev. Lett. **126**, 252501 (2021).

[31] T. Koiwai, K. Wimmer, P. Doornenbal, A. Obertelli, C. Barbieri, T. Duguet, J. Holt, T. Miyagi, P. Navrátil, K. Ogata *et al.*, Phys. Lett. B **827**, 136953 (2022).

[32] T. Kubo, D. Kameda, H. Suzuki, N. Fukuda, H. Takeda, Y. Yanagisawa, M. Ohtake, K. Kusaka, K. Yoshida, N. Inabe *et al.*, Prog. Theor. Exp. Phys. **2012**, 03C003 (2012).

[33] T. Kubo, 14th International Conference on Electromagnetic Isotope Separators and Techniques Related to their Applications, Nucl. Instrum. Methods Phys. Res., Sect. B **204**, 97 (2003).

[34] A. Obertelli, A. Delbart, S. Anvar, L. Audirac, G. Authelet, H. Baba, B. Bruyneel, D. Calvet, F. Château, A. Corsi *et al.*, Eur. Phys. J. A **50**, 8 (2014).

[35] C. Santamaria, A. Obertelli, S. Ota, M. Sasano, E. Takada, L. Audirac, H. Baba, D. Calvet, F. Château, A. Corsi *et al.*, Nucl. Instrum. Methods Phys. Res., Sect. A **905**, 138 (2018).

[36] S. Takeuchi, T. Motobayashi, Y. Togano, M. Matsushita, N. Aoi, K. Demichi, H. Hasegawa, and H. Murakami, Nucl. Instrum. Methods Phys. Res., Sect. A **763**, 596 (2014).

[37] I. Murray, F. Browne, S. Chen, M.L. Cortés, P. Doornenbal, H. Sakurai, J. Lee, M. MacCormick, W. Rodriguez, V. Vaquero *et al.*, RIKEN Accel. Prog. Rep. **51**, 158 (2018).

[38] T. Kobayashi, N. Chiga, T. Isobe, Y. Kondo, T. Kubo, K. Kusaka, T. Motobayashi, T. Nakamura, J. Ohnishi, H. Okuno *et al.*, Nucl. Instrum. Methods Phys. Res., Sect. B **317**, 294 (2013), XVIth International Conference on ElectroMagnetic Isotope Separators and Techniques Related to their Applications, December 2–7, 2012 Matsue, Japan.

[39] ROOT MultiDimFit (accessed August 18, 2022), https://root.cern.ch/doc/master/classTMultiDimFit.html.

[40] Y. Kondo, T. Tomai, and T. Nakamura, Nucl. Instrum. Methods Phys. Res., Sect. B **463**, 173 (2020).

[41] T. Aumann *et al.*, R^{3}B technical design report for NeuLAND, 2011 (accessed September 2022), https://edms.cern.ch/ui/file/1865739/1/TDR_R3B_NeuLAND_public.pdf.

[42] P. Doornenbal, Prog. Theor. Exp. Phys. **2012**, 03C004 (2012).

[43] M. L. Cortés, P. Doornenbal, M. Dupuis, S. M. Lenzi, F. Nowacki, A. Obertelli, S. Péru, N. Pietralla, V. Werner, K. Wimmer *et al.*, Phys. Rev. C **97**, 044315 (2018).

[44] S. Chen, P. Doornenbal, A. Obertelli, T. R. Rodríguez, G. Authelet, H. Baba, D. Calvet, F. Château, A. Corsi, A. Delbart *et al.*, Phys. Rev. C **95**, 041302 (2017).

[45] F. Flavigny, P. Doornenbal, A. Obertelli, J.-P. Delaroche, M. Girod, J. Libert, T. R. Rodriguez, G. Authelet, H. Baba, D. Calvet *et al.*, Phys. Rev. Lett. **118**, 242501 (2017).

[46] M. Lettmann, V. Werner, N. Pietralla, P. Doornenbal, A. Obertelli, T. R. Rodríguez, K. Sieja, G. Authelet, H. Baba, D. Calvet *et al.*, Phys. Rev. C **96**, 011301 (2017).

[47] T. Lokotko, S. Leblond, J. Lee, P. Doornenbal, A. Obertelli, A. Poves, F. Nowacki, K. Ogata, K. Yoshida, G. Authelet *et al.*, Phys. Rev. C **101**, 034314 (2020).

[48] L. Olivier, S. Franchoo, M. Niikura, Z. Vajta, D. Sohler, P. Doornenbal, A. Obertelli, Y. Tsunoda, T. Otsuka, G. Authelet *et al.*, Phys. Rev. Lett. **119**, 192501 (2017).

[49] C. M. Shand, Zs. Podolyák, M. Górska, P. Doornenbal, A. Obertelli, F. Nowacki, T. Otsuka, K. Sieja, J. A. Tostevin, Y. Tsunoda, G. Authelet, H. Baba, D. Calvet, A. Château, S. Chen, A. Corsi, A. Delbart, J. M. Gheller, A. Giganon, A. Gillibert *et al.*, Phys. Lett. B **773**, 492 (2017).

[50] S. Agostinelli, J. Allison, K. Amako, J. Apostolakis, H. Araujo, P. Arce, M. Asai, D. Axen, S. Banerjee, G. Barrand *et al.*, Nucl. Instrum. Methods Phys. Res., Sect. A **506**, 250 (2003).

[51] SUNFLOWER Collaboration (accessed September 2022), https://www.nishina.riken.jp/collaboration/SUNFLOWER/misc/download/simulation.php.

[52] S. Baker and R. D. Cousins, Nucl. Instrum. Methods Phys. Res. **221**, 437 (1984).

[53] I. Antcheva, M. Ballintijn, B. Bellenot, M. Biskup, R. Brun, N. Buncic, P. Canal, D. Casadei, O. Couet, V. Fine *et al.*, Comput. Phys. Commun. **180**, 2499 (2009).

[54] L. Olivier, Nuclear structure in the vicinity of ^{78}Ni: in-beam gamma-ray spectroscopy of ^{79}Cu through proton knockout (accessed September 2022), https://tel.archives-ouvertes.fr/tel-01637435/document.

[55] B. V. Pritychenko, T. Glasmacher, B. A. Brown, P. D. Cottle, R. W. Ibbotson, K. W. Kemper, L. A. Riley, and H. Scheit, Phys. Rev. C **63**, 011305(R) (2000).

[56] B. V. Pritychenko, T. Glasmacher, P. D. Cottle, R. W. Ibbotson, K. W. Kemper, L. A. Riley, A. Sakharuk, H. Scheit, M. Steiner, and V. Zelevinsky, Phys. Rev. C **65**, 061304(R) (2002).

[57] F. Maréchal, T. Suomijärvi, Y. Blumenfeld, A. Azhari, D. Bazin, J. A. Brown, P. D. Cottle, M. Fauerbach, T. Glasmacher, S. E. Hirzebruch *et al.*, Phys. Rev. C **60**, 064623 (1999).

[58] L. A. Riley, D. M. McPherson, M. L. Agiorgousis, T. R. Baugher, D. Bazin, M. Bowry, P. D. Cottle, F. G. DeVone, A. Gade, M. T. Glowacki *et al.*, Phys. Rev. C **93**, 044327 (2016).

[59] F. Nowacki and E. Caurier, Acta Phys. Pol. B **30**, 749 (1999).

[60] E. Caurier, G. Martínez-Pinedo, F. Nowack, A. Poves, and A. P. Zuker, Rev. Mod. Phys. **77**, 427 (2005).

[61] M. Dufour and A. P. Zuker, Phys. Rev. C **54**, 1641 (1996).

[62] T. Baugher, A. Gade, R.V.F. Janssens, S.M. Lenzi, D. Bazin, B.A. Brown, M.P. Carpenter, A.N. Deacon, S.J. Freeman, T. Glasmacher, G.F. Grinyer, F.G. Kondev, S. McDaniel, A. Poves, A. Ratkiewicz, E.A. McCutchan, D.K. Sharp, I. Stefanescu, K.A. Walsh, D. Weisshaar, S. Zhu, Phys. Rev. C **86**, 011305(R) (2012).

[63] O. Sorlin, S. Leenhardt, C. Donzaud, J. Duprat, F. Azaiez, F. Nowacki, H. Grawe, Z. Dombrádi, F. Amorini, A. Astier *et al.*, Phys. Rev. Lett. **88**, 092501 (2002).

[64] N. Bree, I. Stefanescu, P. A. Butler, J. Cederkäll, T. Davinson, P. Delahaye, J. Eberth, D. Fedorov, V. N. Fedosseev, L. M. Fraile *et al.*, Phys. Rev. C **78**, 047301 (2008).

[65] W. Rother, A. Dewald, H. Iwasaki, S. M. Lenzi, K. Starosta, D. Bazin, T. Baugher, B. A. Brown, H. L. Crawford, C. Fransen *et al.*, Phys. Rev. Lett. **106**, 022502 (2011).

[66] T. Wakasa, K. Ogata, and T. Noro, Prog. Part. Nucl. Phys. **96**, 32 (2017).

[67] J. Raynal, Phys. Rev. C **23**, 2571 (1981).

[68] A. Koning and J. Delaroche, Nucl. Phys. A **713**, 231 (2003).

[69] V. R. Brown and V. A. Madsen, Phys. Rev. C **17**, 1943 (1978).

[70] A. Bernstein, V. Brown, and V. Madsen, Phys. Lett. B **103**, 255 (1981).

[71] Z. Elekes, Z. Dombrádi, A. Saito, N. Aoi, H. Baba, K. Demichi, Z. Fülöp, J. Gibelin, T. Gomi, H. Hasegawa *et al.*, Phys. Rev. C **73**, 044314 (2006).

[72] L. Gaudefroy, O. Sorlin, C. Donzaud, J. C. Angélique, F. Azaiez, C. Bourgeois, V. Chiste, Z. Dlouhy, S. Grévy, D. Guillemaud-Mueller *et al.*, Eur. Phys. J. A **23**, 41 (2005).

[73] T. Braunroth, A. Dewald, H. Iwasaki, S. M. Lenzi, M. Albers, V. M. Bader, T. Baugher, T. Baumann, D. Bazin, J. S. Berryman *et al.*, Phys. Rev. C **92**, 034306 (2015).

[74] S. Takeuchi, N. Aoi, T. Motobayashi, S. Ota, E. Takeshita, H. Suzuki, H. Baba, T. Fukui, Y. Hashimoto, K. Ieki *et al.*, Phys. Rev. C **79**, 054319 (2009).

[75] W. Horiuchi, T. Inakura, and S. Michimasa, Phys. Rev. C **105**, 014316 (2022).

[76] H. J. Ong, N. Imai, N. Aoi, H. Sakurai, Z. Dombrádi, A. Saito, Z. Elekes, H. Baba, K. Demichi, Z. S. Fülöp *et al.*, Phys. Rev. C **73**, 024610 (2006).

[77] M. Wang, W. Huang, F. Kondev, G. Audi, and S. Naimi, Chin. Phys. C **45**, 030003 (2021).

[78] A. L. Nichols, B. Singh, and J. K. Tuli, Nucl. Data Sheets **113**, 973 (2012).

[79] E. Browne and J. Tuli, Nucl. Data Sheets **114**, 1849 (2013).